Earth and Space Science

RESEARCH LETTER
10.1029/2020EA001422

Improving Hurricane Boundary Layer Parameterization Scheme Based on Observations

Sundararaman Gopalakrishnan[1], **Andrew Hazelton**[1,2], **and Jun A. Zhang**[1,2]

[1]Hurricane Research Division, NOAA-AOML, Miami, FL, USA, [2]Cooperative Institute for Marine and Atmospheric Studies, University of Miami, Miami, FL, USA

Key Points:

- Different planetary boundary layer parameterization schemes applied to hurricane models produce diverse forecasts of structure and intensity change
- Uncertainty related to some key variables used in the parameterization of eddy diffusivity leads to diverse solutions
- The schemes converge to a similar forecast state if key variables such as mixing length or eddy diffusivity are adjusted based on observations

Supporting Information:

- Supporting Information S1

Correspondence to:

S. Gopalakrishnan, sundararaman.g.gopalakrishnan@noaa.gov

Citation:

Gopalakrishnan, S., Hazelton, A., & Zhang, J. A. (2021). Improving hurricane boundary layer parameterization scheme based on observations. *Earth and Space Science*, *8*, e2020EA001422. https://doi.org/10.1029/2020EA001422

Received 18 SEP 2020
Accepted 6 JAN 2021

Abstract Flight-level data and global positioning system dropwindsonde observations collected from more than 187 flights into 19 tropical cyclones were used to examine why different planetary boundary layer parameterization schemes applied to hurricane models produce diverse forecasts of structure and intensity change. Two popular, yet diverse, physics schemes, namely, the GFS K-Profile and a 1.5-order turbulence kinetic energy closure parameterization from NOAA's next-generation FV3-based Hurricane Analysis and Forecast System were used. It was found that uncertainty related to some key variables used in the parameterization of the eddy diffusivity, K_m, led to diverse solutions. For a given grid resolution, both parameterization schemes converged to a similar forecast state provided those uncertainties could be identified and improved based on observations. This is important for providing a generalized framework for the development and evaluation of parameterization schemes in operational models that resemble reality. This study also indicates that the shape of the K_m profile is equally important as its maximum value. The smaller the K_m near the surface, the stronger the inflow in the boundary layer.

Plain Language Summary Tropical cyclone track and intensity forecasts are sensitive to the physics in atmospheric models. This study investigates why different planetary boundary layer (PBL) parameterization schemes applied to hurricane models produce diverse forecasts of structure and intensity change. Model outputs from NOAA's next-generation, FV3-based, Hurricane Analysis, and Forecast System, along with a wealth of observations from previous Hurricane Field Programs conducted by NOAA, are analyzed. Our results show that uncertainty related to some key variables used in the definition of eddy diffusivity, which represents the strength of vertical turbulent mixing, leads to diverse solutions in model forecasts. However, two diverse PBL parameterization schemes were found to converge to a similar forecast state when key variables such as eddy diffusivity or mixing length were adjusted based on observations.

1. Introduction

Turbulence and mixing within the tropical cyclone (TC) boundary layer control TC structure and intensity change (Gopalakrishnan et al., 2013, 2016). Forecast models operating at horizontal resolutions above a few hundred meters use planetary boundary layer (PBL) schemes to represent the subgrid-scale processes of diffusion and mixing. However, different PBL schemes used in different models, or the same model used in PBL impact assessment studies, have been found to provide a variety of solutions, from rapid intensification (RI) to little or no intensification for the same TC (e.g., Bao et al., 2012; Braun & Tao, 2000; Kepert, 2012; Smith & Thomsen, 2010; J. A. Zhang et al., 2017). Some of these studies have recommended the use of one PBL parameterization scheme over another (e.g., Kepert, 2012). Key questions arising from these studies are why do PBL parameterization schemes diverge so widely from one another? Can we expect some of these PBL parameterization schemes to converge to a similar solution?

In this study, based on a wealth of inner-core observations collected in TCs, we discuss the reasons for the wide divergence between two popular, yet diverse, PBL schemes, namely, a nonlocal K-profile parameterization (KPP) scheme and the turbulent kinetic energy (TKE) scheme used in NOAA's next-generation, FV3-based, Hurricane Analysis and Forecast System (HAFS).

1.1. KPP Scheme

The Operational Global Forecast System (GFS) of the National Centers for Environmental Prediction (NCEP) uses KPP in the well-mixed boundary layer (which includes the hurricane boundary layer), as well as a simple first-order PBL scheme based on the local Richardson number in the stable boundary layer, to determine the eddy diffusivities of momentum (K_m) and heat (K_h). The GFS-PBL scheme has also been a popular option in research models such as the fifth-generation Pennsylvania State University-National Center for Atmospheric Research Mesoscale Model (MM5) and the Weather Research and Forecasting (WRF) model. In 2013, Gopalakrishnan et al. found limitations to the GFS-PBL scheme for TC applications while developing NOAA's high-resolution Hurricane Weather Research and Forecasting (HWRF) model (Bao et al., 2012; Gopalakrishnan et al., 2011, 2012, 2013). Flight-level data collected by a NOAA WP-3D research aircraft during eyewall penetrations of category 5 hurricanes Allen (1980) and Hugo (1989) were used as the basis to best match the modeled eddy diffusivities with wind speed. The authors included an alpha (α) parameter to the nonlocal K approach valid within the well-mixed boundary layer. In this scheme, the momentum eddy diffusivity is

$$K_m = k\left(U_* / \Phi_m\right) Z\left[\alpha\left(1 - Z / h\right)^2\right] \tag{1}$$

where k is the von Karman constant (0.4), U_* is the surface frictional velocity scale, Φ_m is the wind profile function evaluated at the top of the surface layer, Z is the height above the surface, and h is the depth of the turbulent PBL (also known as the mixed layer[1]) that is, determined based on the height above the ground at which the bulk Richardson number exceeds a critical value of 0.25. In the original formulation, which may be valid over land, $\alpha = 1$, and K_h is computed from K_m using the relationship of the Prandtl number (Hong & Pan, 1996).

A reduction in the eddy diffusivity to a quarter of its original value (i.e., $\alpha = 0.25$) produced the best match with the observations of K_m and also revealed a marked decrease in the inflow layer depth in HWRF, more consistent with observations (S. G. Gopalakrishnan et al., 2013). This, in turn, drastically affected the size and intensity changes in the modeled TC. For the first time, idealized simulations of HWRF reproduced the TC spin-up mechanism consistent with theoretical findings (e.g., Montgomery & Smith, 2014; Smith et al., 2009). Application of the modified scheme with $\alpha = 0.50$ to the operational HWRF model improved size predictions by almost 50% (Tallapragada et al., 2014) and had a significant impact on intensity forecasts (J. A. Zhang et al., 2015). However, as mentioned in S. G. Gopalakrishnan et al. (2013), models such as the GFS and HWRF use an admittedly simplified parameterization; the study recommended the use of higher-order PBL schemes for TC predictions.

1.2. TKE Scheme

An improvement over the bulk scheme is the use of TKE for describing eddy diffusivity (e.g., J. Han & Bretherton, 2019). In this scheme, the momentum eddy diffusivity is

$$K_m = clE^{0.5} \tag{2}$$

where c is a constant (0.4), l is the mixing length, and E is the TKE. In its simplest form, TKE is predicted by a prognostic equation that includes shear production, buoyancy production (or destruction), turbulence transport and the dissipation of TKE, and prognosed mixing length (e.g., J. Han, 2015; J. Han & Bretherton, 2019; Sharan & Gopalakrishnan, 1997; Stull, 2000; Yamada & Mellor, 1975). The dissipation term in

[1]A definition of the height of the PBL in hurricanes is an area of debate. There is no consensus on what should define this height (J. A. Zhang et al., 2011b). Estimation and mapping of hurricane turbulent energy using airborne Doppler measurements (Lorsolo et al., 2010) shows that significant mixing in the eyewall can occur even at 10 km height. At the same time, several other authors use inflow layer depth, which is about 1 km from the surface, as the height of the dynamical boundary layer. In forecast models where the model top extends to 10 MB or less, the height of the boundary layer, h, evolves both in time and space with the evolving dynamics and thermodynamics of the model. So, we avoided any assumptions related to any of these characteristic height scales related to the PBL and let the model evolve in time and space, and compared the scale heights from the model with observations.

the TKE budget equation is parameterized as $0.714E^{3/2}/l_d$. The most generalized form of mixing length is defined by

$$1/l = 1/l_1 + 1/l_2 \quad (3)$$

where l_d, l_1, and l_2 are, respectively, the mixing length scales for dissipation, at the surface and PBL. l_d is usually related to l. Although the TKE equation has a strong physical basis, the definition of the mixing lengths in these schemes for numerical models has been an active topic of research. In almost all formulations, mixing length, l_1, is assumed to linearly increase with height while l_2 is the saturation factor. Depending on the application, the definition of l_2 has varied from simple dependency on geostrophic wind above the stable boundary layer (e.g., Sharan & Gopalakrishnan, 1997) to more complex formulations for modeling diurnal variations over flat land or complex terrain (Bougeault & Lacarrère, 1989; Therry & Lacarrère, 1983). Bougeault and Lacarrère (1989) related the length scale l_2 to the distance that a parcel having an initial TKE can travel upward and downward before being stopped by buoyancy effects. More recently, Kepert (2012) used a boundary layer model to study the impacts of various PBL schemes on the TC structure predictions. The study used a range of values for l_2 starting from 40 to 300 m and found that increasing l_2 leads to higher diffusivity in the middle to upper part of the inflow layer. However, it should be noted that none of these formulations for l_2 used observed values. This motivated us to review hurricane observations collected during eyewall penetrations of major hurricanes Allen (1980), Hugo (1989), and Frances (2004) at an altitude of about 450–500 m to estimate l_2. Using the methodology discussed in Tang et al. (2018) it was found that the maximum value of l_2 did not exceed 100 m, whereas the original default was 300 m in the J. Han and Bretherton (2019) formulation.

2. Observations

Both real-time observations from Hurricane Michael (2018) as well as a wealth of data from several other hurricanes are used in this study. Flight-level data collected by a NOAA WP-3D research aircraft during eyewall penetrations of major hurricanes Allen (1980), Hugo (1989), and Frances (2004) at an altitude of about 450–500 m was used to estimate the observed eddy diffusivity as a function of wind speed. In addition, an analysis of near-surface (10 m) inflow angles using wind vector data and mean radius-height structure from more than 1,800 quality-controlled dropsondes deployed by aircraft on 187 flights in 19 hurricanes were used as a basis to develop a composite framework for observations (J. A. Zhang et al., 2011a; J. A. Zhang & Uhlhorn, 2012). Such a framework has proven to be very useful for model comparisons (e.g., S. G. Gopalakrishnan et al., 2013; Hawkins & Imbembo, 1976; Powell et al., 2003; J. A. Zhang et al., 2017). Different aspects of these composite structures are documented in detail by J. A. Zhang et al. (2011b, 2013). Surface inflow angle is an important dynamical parameter for the boundary layer because it measures the relative strength of the tangential and radial winds that control the primary and secondary circulations in TCs (Bryan, 2012). In the composite framework discussed here, data were grouped as a function of the radius to the storm center normalized by the radius of maximum wind speed (RMW), where RMW was defined as the radius of maximum axisymmetric wind speed at 2 km altitude. NOAA P-3 Tail Doppler Radar (TDR) analysis from observations obtained in real-time during Hurricane Michael (2018) were also used for evaluation (Fischer et al., 2020). The TDR analysis and quality control procedures with examples are described in Rogers et al. (2012) and Reasor et al. (2013).

3. Model

The HAFS is NOAA's next-generation multiscale, atmosphere-ocean coupled numerical model and data assimilation package for TCs, supported by the Hurricane Forecast Improvement Program (HFIP; Gopalakrishnan et al., 2019). The model is based on the FV3 dynamic core and is part of the Unified Forecast System (UFS) under development. A baseline version of HAFS was created at NOAA's Atlantic Oceanographic and Meteorological Laboratory (AOML) in collaboration with NCEP's Environmental Modeling Center and run during the 2019 hurricane season as a part of the HFIP demonstration experiment (A. T. Hazelton et al., 2020a, 2020b). The model configuration here uses a large static nest covering the entire Atlantic basin at ~3-km horizontal grid spacing (Harris & Lin, 2013; A. T. Hazelton et al., 2018, 2020a, 2020b) within the global model (at ~12–13 km horizontal grid spacing). Recently, A. T. Hazelton et al. (2020a) studied the RI

Table 1
Experimental Simulations of a Hurricane

No.	Name	Description	Parameter
1	EDMF-GFS	Original EDMF-GFS	$\alpha = 1$
2	EDMF-TKE	Original EDMF-TKE	max $(l_2) = 300$ m
3	MEDMF-GFS	Modified EDMF-GFS	$\alpha = 0.25$
4	MEDMF-TKE	Modified EDMF-TKE	max $(l_2) = 100$ m
5	M2EDMF-GFS	HWRF-GFS scheme	$\alpha = 0.50$

of Hurricane Michael (2018) using an ensemble of HAFS global-nested runs. The same initialization of 18:00 UTC October 7, 2018 was used for this study.

Two different PBL options were used: (1) the GFS-PBL scheme (S. G. Gopalakrishnan et al., 2013; J. Han & Pan, 2011; Hong & Pan, 1996), which was recently upgraded with the introduction of an eddy-diffusivity mass-flux (EDMF) term to account for the growth of countergradient fluxes on top of the mixed layer over land (J. M. Han et al., 2016); and (2) a 1.5-order TKE scheme with EDMF corrections. An excellent documentation of the implementation of this new TKE scheme in the FV3 model is provided in J. Han (2015) and J. Han and Bretherton (2019).

The eddy diffusivity defined in the EDMF-GFS were altered by using $\alpha = 0.25$ and 0.5 (Gopalakrishnan, 2013) in Equation 1 and the maximum of l_2 in Equation 3 was set to 100 m in the EDMF-TKE. Although the choice of the numbers was based on observations, it should be noted that these are notional values chosen to explain the diversity in the results that changes to the parameterization schemes can produce. Changes to the PBL schemes were made in both the global and the nested domains. The list of simulations conducted in this study is shown in Table 1. All other parameterization schemes were kept the same as reported in A. T. Hazelton et al. (2020a), except for a change in the surface exchange coefficients (e.g., Bender et al., 2007) which were set to be similar to HWRF (S. G. Gopalakrishnan et al., 2013).

4. Results

Figure 1 illustrates how for the same simulation of Hurricane Michael two different schemes or simple changes to a PBL scheme produces diversity in both tracks (Figure 1a) and intensity (Figure 1b). The EDMF-GFS scheme produces the weakest TC, failing to reproduce RI (Figure 1b); nevertheless, the track forecast, until landfall, is more consistent with the best track (Figure 1a). On the contrary, the MEDMF-GFS scheme produces RI more consistent with the observations (Figure 1b) but produces a significant divergence in track (Figure 1a). Both runs from the TKE scheme, i.e., EDMF-TKE and MEDMF-TKE, produce a more consistent track and intensity forecast, closer to the best track.

Figure 2 provides an overall picture of the evolution of the mean tangential wind in Hurricane Michael. The figure demonstrates the performance of the HAFS in forecasting the modeled RI with the different parameterization schemes, as compared to the TDR analyses from observations collected in real-time during the hurricane. Although all of the PBL schemes produce a weaker vortex than the observations at 00:00 UTC

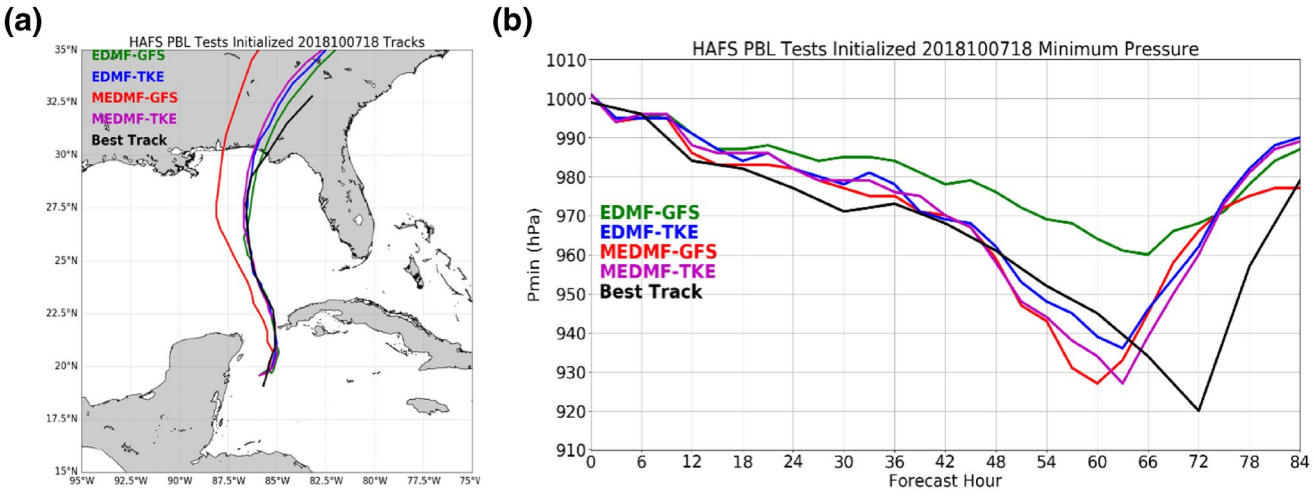

Figure 1. Five-day forecast of (a) tracks and (b) mean sea level pressure for Hurricane Michael initialized at 18:00 UTC October 7, 2018 for the EDMF-GFS, EDMF-TKE, MEDMF-GFS, and MEDMF-TKE PBL parameterization schemes. The observed track (best track) is shown in black.

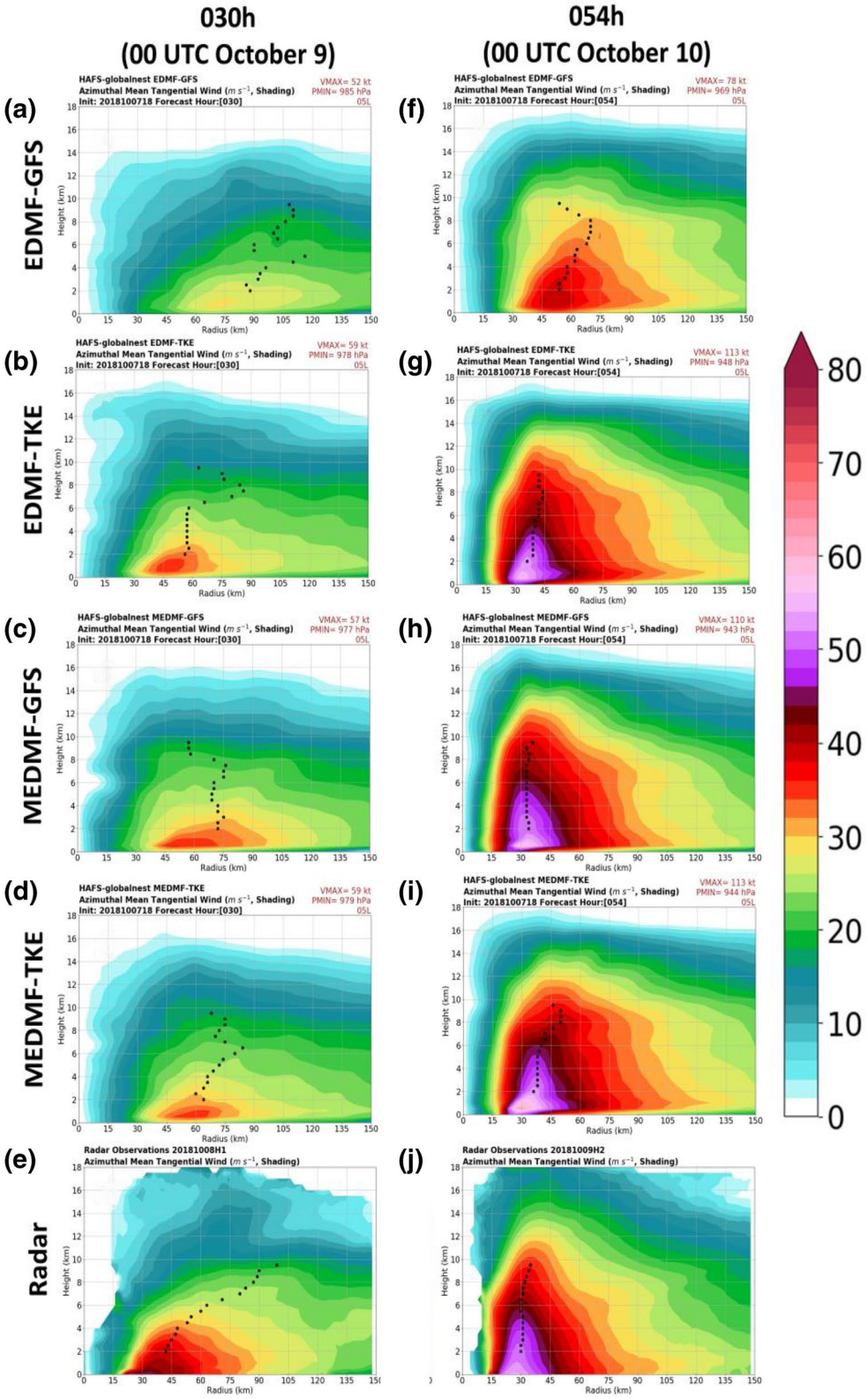

Figure 2. Mean tangential wind structure for the EDMF-GFS, EDMF-TKE, MEDMF-GFS, and MEDMF-TKE PBL parameterization schemes from the HAFS simulations compared to TDR analysis from observations collected in real-time during Hurricane Michael, (a–e) 00:00 UTC October 9, and (f–j) 00:00 UTC October 10. The dotted lines indicate the radial location of maximum wind at a given height.

on October 9, with the exception of the EDMF-GFS PBL scheme (Figures 2a and 2f), all other schemes reproduce the RI of Michael 24 h later, consistent with the observations. All schemes show the maximum wind near the surface, i.e., within the lower 1 km. Additionally, as indicated by the dotted lines showing the location of the RMW at a given height, the vortex is ill-defined at the start of RI (Figures 2a–2e). With the exception of the EDMF-GFS scheme, however, the simulated hurricane vortex is well aligned with height 24 h later in all the schemes (Figures 2g–2i) and is consistent with the TDR observations (Figure 2j). When the eyewall is well established at 00:00 UTC on October 10, the MEDMF-GFS (Figure 2h) and MEDMF-TKE (Figure 2i) schemes have an RMW of ~30–35 km, which is closer to the TDR analysis. The EDMF-GFS scheme has a large RMW, about 50 km (Figure 2f), and even the default EDMF-TKE (Figure 2g) scheme has too large of an RMW (about 40 km). However, it should be noted that TDR analysis from one case may be uncertain, especially near the surface where the inflow (radial wind) becomes critical. While the mean evolution of the analyzed TDR vortex, when available, can be used as a baseline for comparing model performance, composites from observations may be more useful for further generalization of the results.

To understand why the forecast solutions for Hurricane Michael obtained from the four simulations are different (Table 1), the observed composites of K_m (Figure 3a) and surface inflow angle (Figure 3b) were compared with the modeled outputs at the 54th hour during the RI phase when the hurricane was at its strongest and closest to the truth (Figures 1b and 2f–2j). Clearly, EDMF-GFS is the most diffusive scheme, followed by EDMF-TKE. Both of the modified schemes are far less diffusive, with the MEDMF-TKE being the least diffusive scheme (Figure 3a). The modifications produced diffusivities closer to the observed values (black marks in Figure 3a) than the original KPP scheme. At the same time, the simulated inflow angles in the TKE runs were much closer to observations than those in the KPP runs (Figure 3b).

Some studies (Bu et al., 2017; Wang et al., 2018; J. A. Zhang et al., 2015; Kepert, personal communication) have pointed out that inclusion of the α term in the EDMF-GFS schemes to the description of K_m creates inconsistencies, especially near the lower boundary because wind behavior may violate the surface layer similarity profiles in such cases. Bu et al. (2017) introduced a wind speed and Wang et al. (2018) introduced height dependency on α to offset this issue. Indeed, the evaluation of surface inflow angle (Figure 3b) shows that stronger than normal gradients can develop for $\alpha = 0.25$ in the MEDMF-GFS. On the contrary, the original EDMF-GFS scheme creates gradients that are too weak, which implies weak convergence near the surface and a weaker storm, consistent with Figures 1b, 2a, and 2f. Both TKE schemes match better with the observations than the KPP schemes.

Figure 4 demonstrates the impact of eddy diffusivity on TC structure predictions. The figure depicts the azimuthal mean hurricane boundary layer structure from the model simulations (Table 1; experiments 1–4) for 54–60 h and compares this structure with the observational composites obtained from a typical hurricane

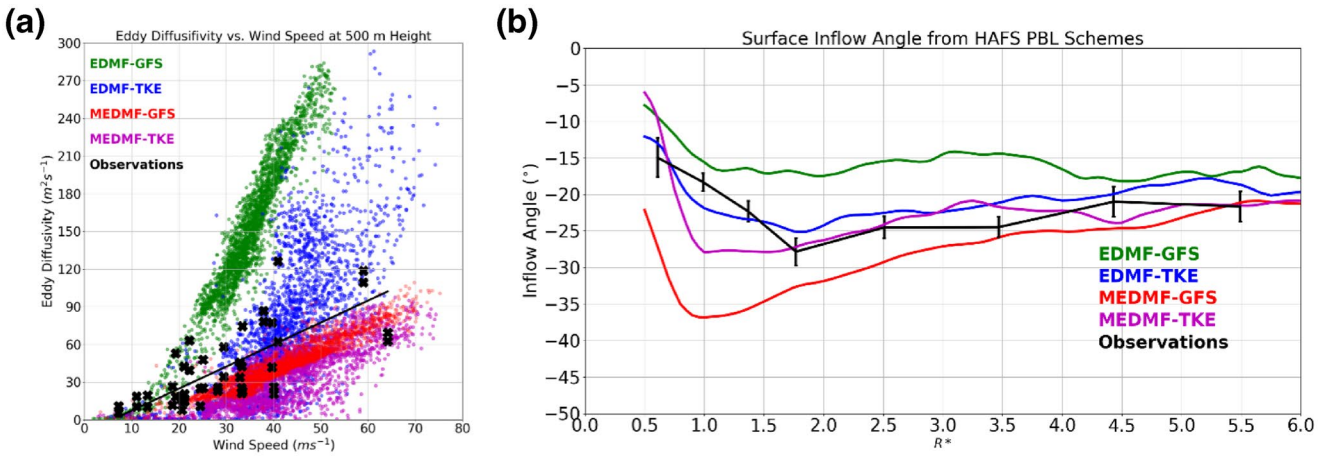

Figure 3. Variations of (a) eddy diffusivity (K_m) with wind speed at 500 m from the HAFS simulations compared with flight-level data from J. A. Zhang et al., (2011a) and (b) plot of surface inflow angle as a function of radius with respect to the storm center normalized by the radius of maximum wind speed from HAFS compared with observations from J. A. Zhang and Uhlhorn (2012) for the EDMF-GFS, EDMF-TKE, MEDMF-GFS, and MEDMF-TKE PBL parameterization schemes.

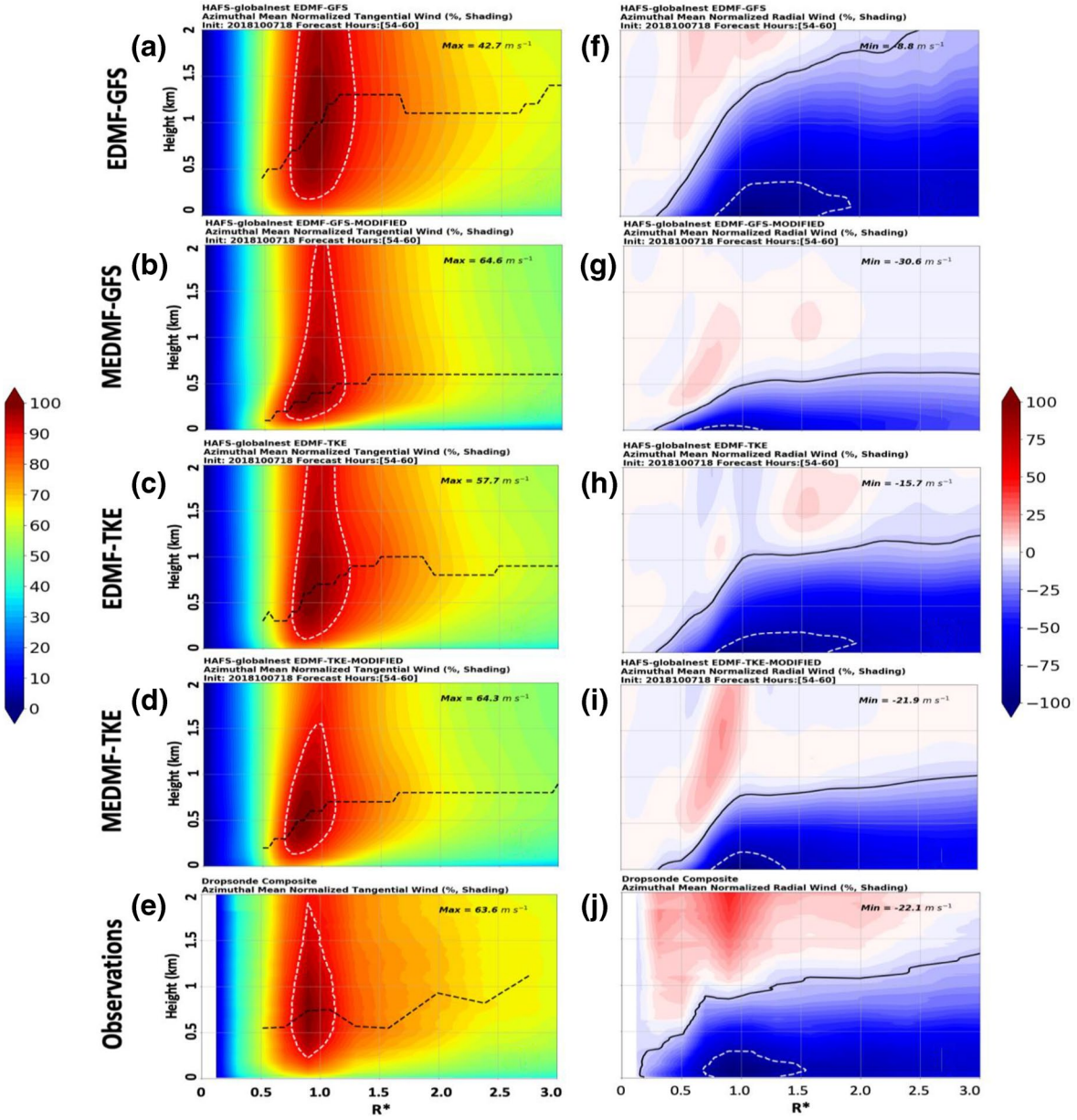

Figure 4. Left panel: Azimuthally averaged tangential wind normalized by the maximum azimuthal mean value (%) as a function of radius normalized by the radius of maximum winds for (a–d), the four runs in Table 1, and (e) observed composites from J. A. Zhang et al. (2015). In (a–e) the white dashed contour represents the core of hurricane wind containing 90% of the maximum tangential wind, and the black dashed line shows the height of the tangential wind peak at each radius. Right panel: Azimuthally averaged radial wind normalized by the maximum azimuthal mean value (%) as a function of radius normalized by the radius of maximum winds for (f–i), the four runs in Table 1, and (j) observed composites from J. A. Zhang et al. (2015). In (f–j) the white dashed contour represents the core of inflow containing 80% of the maximum radial wind, and the black line shows the depth of the inflow layer where radial wind diminishes to 90% of its peak value.

like Michael (J. A. Zhang et al., 2015). To further facilitate a one-on-one comparison with the observations, the tangential (left panel) and radial winds (right panel) were normalized by their respective peak values for analyzing the overall structure. For the EDMF-GFS scheme, a core of hurricane wind comprising 90% of the maximum wind extends well above 2,000 m altitude (Figure 4a). The peak is reduced closer to observations in the run with MEDMF-GFS (Figure 4b), and the height of the maximum tangential wind is also lowered. The EDMF-TKE scheme (Figure 4c) has the core region closer to observations (Figure 4e) than EDMF-GFS, but the MEDMF-TKE (Figure 4d) further improves the structure such that this scheme produces the result that is, closest to the observations (Figure 4e). A comparison between the model simulations of maximum

tangential wind indicates that EDMF-GFS produces the weakest storm with a maximum wind of 42.7 m s^{-1} (Figure 4a), whereas both modified schemes produce a category-4 storm (Figures 4b and 4d).

Examining the normalized radial flow for the EDMF-GFS scheme with no modifications, the inflow layer is much too deep and weak (Figure 4f). This is significantly changed in the MEDMF-GFS run, but perhaps produces too shallow and too strong an inflow layer (Figure 4g). For the EDMF-TKE, the unmodified forecast shows a PBL inflow structure that is, still slightly too deep, with a depth >1,000 m at the RMW (Figure 4h). The structure in the MEDMF-TKE (Figure 4i) is closer to the observed inflow depth of about 700–800 m (Figure 4j) at $R^* = 1$. Another key difference in the radial flow is the location of the radial inflow maximum (denoted by the 80% contour). In more diffusive schemes (Figures 4f and 4h), the inflow peak extends from $R^* = 1$–2. However, with reduced diffusivity (Figures 4g and 4i), the peak inflow is closer to observations around $R^* = 1$ that extends farther inside the RMW. This has implications for intensity change, promoting more influx of absolute angular momentum inside the RMW and subsequent vortex spin-up (e.g., Montgomery & Smith, 2014), as well as enhanced convergence inside the RMW, which tends to promote stronger updrafts above the PBL (e.g., Ahern et al., 2019; J. A. Zhang et al., 2017).

Figure 5 illustrates the effect of eddy diffusivity on the TC intensification process. The azimuthally averaged radius-height cross-section of K_m indicates that the amount of diffusion modulates both the inflow layer depth and strength of the inflow and, consequently, the inflow angle (Figure 3b). S. G. Gopalakrishnan et al. (2013) found that larger diffusion in a deeper layer negated the gradients between the surface layer and the PBL, leading to weaker frictional forces and weaker inflow. On the contrary, a reduction in diffusion strength leads to shallow, but stronger frictional forces, a larger gradient wind imbalance in the boundary layer, and stronger radial acceleration (deceleration) in the eyewall region which, in turn, leads to enhanced PBL inflow and enhanced vortex spin-up in the PBL (refer to Equations 2 and 3 in S. G. Gopalakrishnan et al. [2013]). It also leads to enhanced convergence in the PBL, convection in the eyewall and, subsequently, enhanced feedback to the PBL inflow and a stronger hurricane. S. G. Gopalakrishnan et al. (2013) found that the radial acceleration of the inflow not only produced a stronger outflow at the top of the inflow layer,

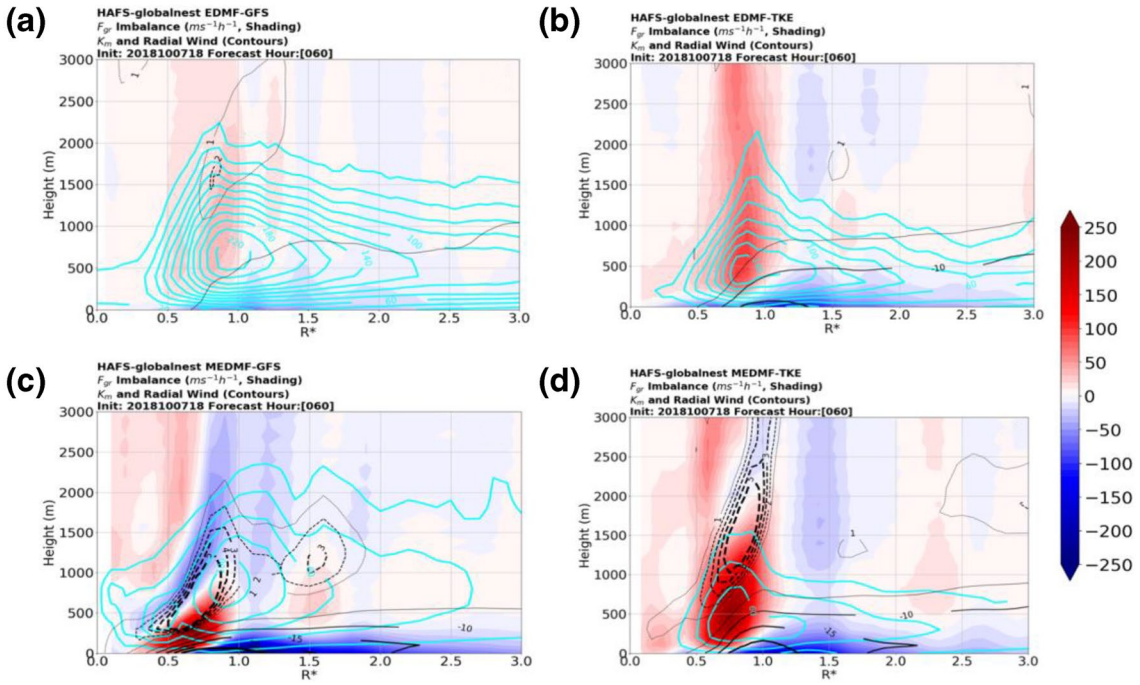

Figure 5. Azimuthally averaged, time-averaged, radius-height cross section of eddy diffusivity (K_m) centered around 60 h depicted by cyan contours for the (a) EDMF-GFS, (b) EDMF-TKE, (c) MEDMF-GFS, and (d) MEDMF-TKE PBL. Superposed in color are the forcing terms related to gradient wind imbalance within the boundary layer (S. G. Gopalakrishnan et al., 2013). Units of the forcing term are in m s^{-1} h^{-1}. The inflow is shown by solid black lines, whereas outflow is shown as dashed black contours.

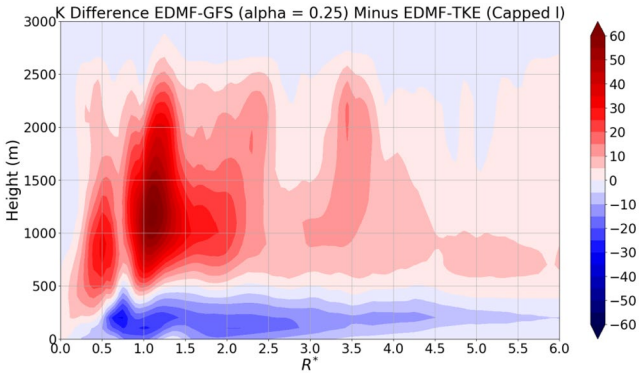

Figure 6. Difference in K_m between MEDMF-GFS and MEDMF-TKE PBL.

more consistent with observations, but also a smaller inner core and a more compact TC. These processes are on display in the simulations of Hurricane Michael.

The core of maximum eddy diffusivity of about 220 $m^2\ s^{-1}$ for the EDMF-GFS scheme is located between 500 and 1,000 m height at $R^* = 1$ (Figure 5a). The EDMF-GFS produces the weakest frictional forces, with weaker gradient wind imbalances within a thicker inflow layer that result in weaker radial acceleration and, consequently, a weaker hurricane (Figures 1b, 2a and 2f). The core of maximum eddy diffusivity of about 140 $m^2\ s^{-1}$ for the EDMF-TKE scheme is located at about 500 m height and $R^* = 0.5–1$ (Figure 5b). The scheme produces a shallower inflow layer with stronger radial acceleration of the inflow and, subsequently, the maximum speed of radial wind is nearly doubled (about 16 $m^2\ s^{-1}$) when compared to EDMF-GFS (Figures 4f and 4h). However, in these cases the gradient wind imbalance and subsequent radial acceleration are not strong enough to erupt a strong outflow above the inflow layer. Further reduction of K_m in the modified schemes (Figures 5c and 5d) leads to a further increase in the frictional force, creating a larger imbalance in the gradient wind, acceleration of flow within the inflow layer, and a significant eruption of the outflow. The outflow above the inflow layer in the eyewall is on the order of 3–5 m s^{-1} (Figures 5c and 5d), and the maximum inflow speed in the MEDMF-GFS and MEDMF-TKE are, respectively, 31 and 21 m s^{-1} (Figures 4g and 4i). However, why are the two modified schemes different in terms of those maximum inflow speeds?

Figure 6 demonstrates the impact of the shape of the K_m-profile on the strength of the inflow. While the influence of eddy diffusivity on TC intensification is generally consistent with S. G. Gopalakrishnan et al. (2013) and J. A. Zhang et al. (2015), the height dependence of the K_m profile was largely ignored in those studies because only one scheme, namely, the GFS PBL was used. The authors modified the α value (i.e., they used 1.0, 0.5, and 0.25), wherein the K_m profiles were fixed and only maximum values were systematically altered. However, there are differences in K_m between the MEDMF-GFS and MEDMF-TKE schemes (Figures 5c and 5d). The difference plot between MEDMF-GFS and MEDMF-TKE (Figure 6) shows that, although the maximum eddy diffusivity is larger than 100 $m^2\ s^{-1}$ for the MEDMF-GFS (Figure 5c) compared to about 60 $m^2\ s^{-1}$ for the MEDMF-TKE (Figure 5d), there is more diffusion in the inflow region below 500 m and less above the inflow layer in the latter scheme (Figure 6). Subsequently, the maximum inflow is reduced in the MEDMF-TKE compared to MEDMF-GFS, producing a structure closer to the observations (Figures 4i and 4j).

Finally, to address the question of whether two different PBL schemes can converge to the same solution, an additional simulation with EDMF-GFS for $\alpha = 0.5$ was used (Table 1). Figure 7a depicts the variations of eddy diffusivity (K_m) with wind speed at 500 m from the HAFS simulations compared with flight-level data from J. A. Zhang et al. (2011a) for the relevant schemes in this discussion. Figure 7b plots the corresponding surface inflow angle as a function of radius with respect to the storm center normalized by the radius of maximum wind speed from HAFS compared with observations from J. A. Zhang and Uhlhorn (2012). Figure 7a indicates the M2EDMF-GFS scheme behaves closer to the EDMF-TKE scheme, especially at higher wind speeds. Indeed, larger diffusion, especially in the eyewall region (Figure 7a) also reduces the anomalous super gradient wind in the eyewall region with the M2EDMF-GFS scheme (Figure 7b).

The 500-hpa height is usually referred to as a steering level because strong hurricanes roughly move in the same direction as the wind at this level. Figure 8 depicts the difference in the 500-hpa height field at the 48th hour between the MEDMF-GFS and M2EDMF-GFS schemes. It is clearly observed that the difference in the height field between the two schemes is restricted to the inner core and a small area near Florida. Strong inflow observed in the MEDMF-GFS scheme ($\alpha = 0.25$; Figure 7b) produces significant changes to the inner core vortex structure and, subsequently, its interactions with the large-scale environment around the hurricane (Figure 8a). On the contrary, the M2EDMF-GFS scheme behaves very similar to the EDMF-TKE scheme, leading not only to a similar vortex but to also a similar large-scale environment as in the case of the EDMF-TKE. The net effect is observed in the convergence of the tracks for Hurricane Michael

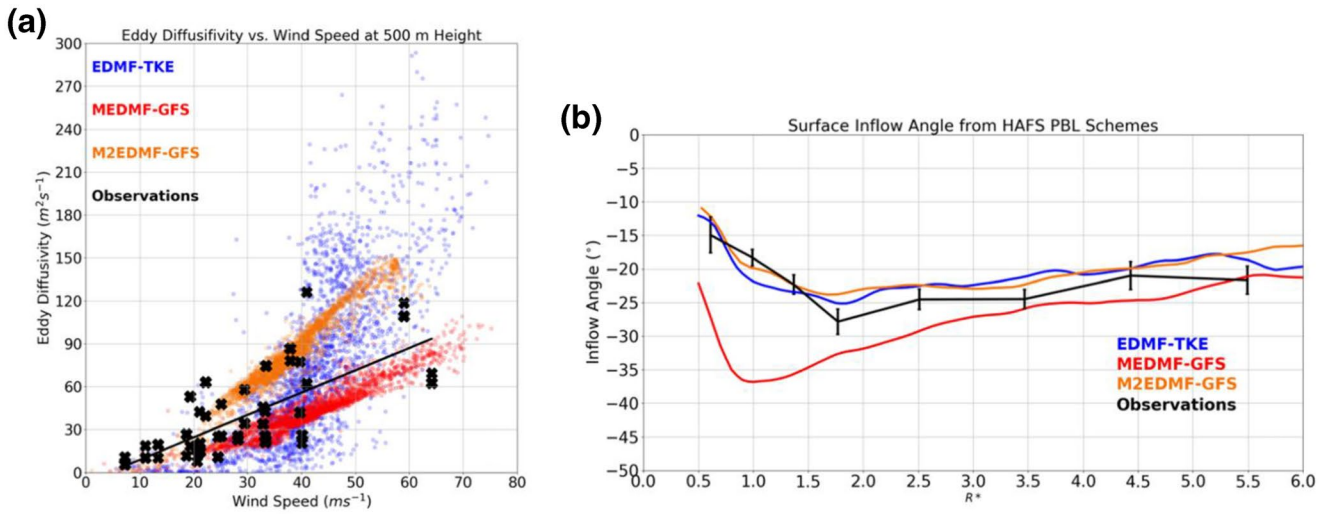

Figure 7. (a and b) are the same as Figures 3a and 3b but for an additional simulation of $\alpha = 0.5$.

(Figure 8b). As expected, the intensity forecast from this simulation is also closer to the EDMF-TKE scheme than either the MEDMF-GFS ($\alpha = 0.25$) or the original GFS scheme (Figure 8c).

It must be emphasized that while some generalization could be made with a certainty of the impact of eddy diffusivity (Figures 3a and 7a) on TC structure (Figures 4 and 5) and intensity predictions (Figures 1b and 8c), understanding its impact on track behavior is nontrivial. Hurricane Michael represents a near-ideal case where changes to the KPP (for $\alpha = 0.25$) produced stronger and anomalous inflow (Figures 3b and 7b) within the hurricane inner core region (Figure 8a) that directly influenced the tracks (Figure 8b). However, large gradients of wind velocities are known to occur in frontal zones away from the hurricanes and over the land areas. The impact of eddy diffusivity is unknown in those regions. Although the PBL changes were implemented in both the global model as well as the embedded high-resolution static nest, and yet, major changes were restricted to the hurricane region for this case, cause and effect relationships cannot be easily generalized in cases where the flow downstream becomes more complex. Besides, many PBL schemes including the GFS KPP and TKE schemes used in global forecast models optimize parameters based on large-eddy simulations of daytime unstable PBL. Therefore, the reduction of K_m (which is suitable for the hurricane PBL) may cause an underestimation of the daytime PBL growth in the regions outside of the

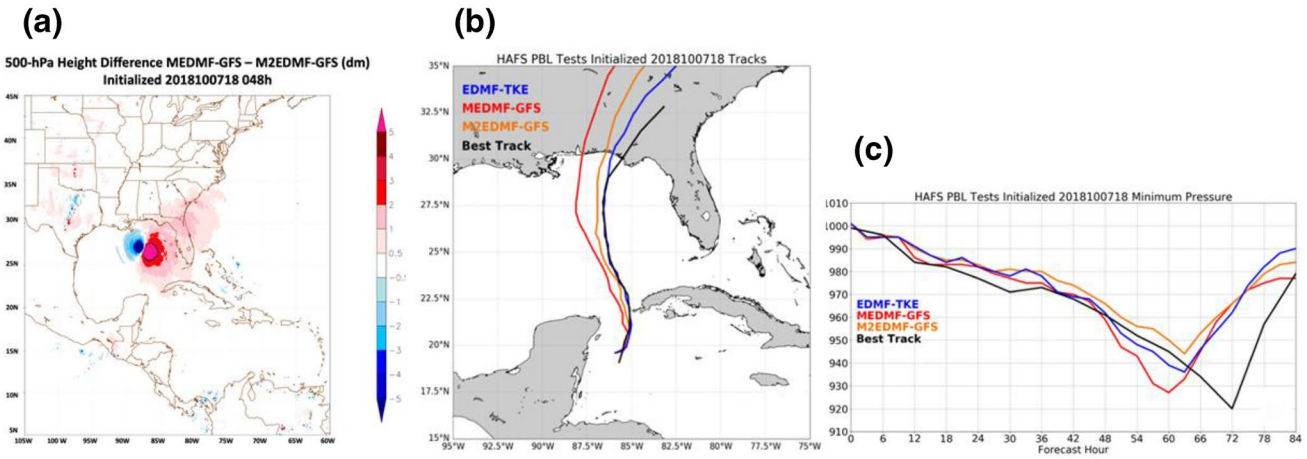

Figure 8. (a) Five-hundred-hpa height difference at the 48th hour between the MEDMF-GFS and M2EDMF-GFS schemes, (b) tracks, and (c) mean sea level pressure for Hurricane Michael initialized at 18:00 UTC October 7, 2018 for the EDMF-TKE, MEDMF-GFS, and M2EDMF-GFS PBL parameterization schemes.

hurricane, which could degrade the forecast of the environmental steering flows and as a result, can lead to degradation of hurricane track forecast in some other cases. Storm centric moving nest for HAFS is under development (HFIP; Gopalakrishnan et al., 2019). Changes to the parameterization schemes suggested here may be implemented only in the moving nest so that the above issues could be avoided while operating a unified forecasting system.

5. Conclusions

Different PBL parameterization schemes applied to hurricane models are known to produce diverse forecasts of structure and intensity change. Two PBL schemes, namely, a relatively simple predefined K-Profile and a 1.5-order TKE closure parameterization from NOAA's next-generation, FV3-based, HAFS and a wealth of observations from Hurricanes Field Programs were used to understand this issue. It was found that inaccuracies related to the parameterization of eddy diffusivity (K_m) in the PBL formulations resulted in a diversity in TC intensity and structure forecasts. However, with minor modifications to the PBL parameterization schemes based on observations, the behavior of the two K-theory-based schemes converged toward reality. While several earlier studies found such divergences in model solutions, to the best of our knowledge, this is the first study to show how two different schemes can converge to the same solution. We believe that is an important step toward advancing a unified parameterization scheme for NOAA's UFS currently under development.

Although our study was restricted to one case, the methodology we adopted is quite general. In fact, the current work builds upon a previous idealized HWRF study by S. G. Gopalakrishnan et al. (2013) and several real-case HWRF studies (e.g., J. A. Zhang et al., 2017). The results from our study indicate that more diffusion in the eyewall region of the hurricane boundary layer negates gradients within the boundary layer and, subsequently, leads to weaker inflow and a weaker TC. Smaller diffusion leads to stronger frictional forces, a stronger acceleration of inflow, and a stronger TC, consistent with observations that are also consistent with S. G. Gopalakrishnan et al. (2013). More importantly, the current work further illustrates that the shape of the K_m profile is as important as its maximum value, i.e., the stronger the K_m in the lower 500 m, the weaker the inflow and vice-versa.

Within the constraint of the available NOAA computing we ran about 42 real cases (21 named TCs that included Tropical Depressions, storms and hurricanes) using the global model and embedded 3-km nest with the same configuration as the one presented in this work with EDMF-TKE and MEDMF-TKE schemes. These 42 cases were chosen from the 2016–2019 season and consisted of both weak and strong storms. We found that while the modified PBL TKE scheme based on observations had minimal, yet, positive impact on the tracks, the absolute error of intensity forecast was substantially reduced at the first 60 h lead time compared to those with the original scheme. Nevertheless, additional case studies may be required to validate our findings especially for track predictions.

Understanding the uncertainty related to the key variables that determine the eddy diffusivity may also be important for developing physics-based ensembles. In other words, the use of perturbations in the mixing length, for example, in a TKE scheme may provide a more reasonable spread in ensembles than using multiple PBL schemes. In fact, HWRF physics-based ensembles (Zhan et al., 2014) use perturbations to known parameters that are found to be sensitive in the GFS parameterization scheme. While the current study is restricted to hurricanes, a similar approach might also be adopted for the UFS in creating a generalized framework for the PBL parameterization scheme based on observations.

It should be mentioned that our study was limited to sensitivity experiments to the mixing length definition for the EDMF-TKE scheme. For this study, the mixing length that relates the scale to the distance that a parcel having an initial TKE can travel upward and downward before being stopped by the buoyancy effect, was capped. An improved definition of mixing length based on observations for the hurricane boundary layer may be required. Although our study did not focus on the dissipation length scale, this is another important scale that relates the production of TKE to its dissipation of kinetic energy near the surface. Both the mixing length and dissipation length scales need to be parameterized based on observations. The framework presented here could be extended to improve the TKE parameterization scheme in the future for the UFS.

Data Availability Statement

The full modeling data and graphics presented in this work is available at NOAA's R&D supercomputer Hera machine at/scratch2/NAGAPE/aoml-hafs1/Andrew.Hazelton/grl_pbl_data.tar.gz. The data set is about 263 GB and is available to anyone with access to NOAA's R&D supercomputer. That data can also be made available to anyone outside NOAA that makes a request for transfer.

Acknowledgments
The authors acknowledge NOAA's HFIP and the 2019 NOAA Hurricane Supplemental funds for HAFS developments. Credit is due to Drs. Xiaomin Chen and Frank Marks of the Hurricane Research Division of AOML for providing a thorough internal review of the manuscript. Thanks are also due to Ms. Gail Derr for offering excellent editorial support. The authors wish to thank the three reviewers for some insightful comments that led to substantial improvements to the manuscript.

References

Ahern, K., Bourassa, M. A., Hart, R. E., Zhang, J. A., & Rogers, R. F. (2019). Observed kinematic and thermodynamic structure in the hurricane boundary layer during intensity change. *Monthly Weather Review*, *147*(8), 2765–2785. https://doi.org/10.1175/MWR-D-18-0380.1

Bao, J.-W., Gopalakrishnan, S. G., Michelson, S. A., Marks, F. D., Jr., & Montgomery, M. T. (2012). Impact of physics representations in the HWRFX on simulated hurricane structure and pressure-wind relationships. *Monthly Weather Review*, *140*(10), 3278–3299. https://doi.org/10.1175/MWR-D-11-00332.1

Bender, M. A., Ginis, I., Tuleya, R., Thomas, B., & Marchok, T. (2007). The operational GFDL coupled hurricane-ocean prediction system and a summary of its performance. *Monthly Weather Review*, *135*(12), 3965–3989. https://doi.org/10.1175/2007MWR2032.1

Bougeault, P., & Lacarrère, P. (1989). Parameterization of orography-induced turbulence in a mesobeta-scale model. *Monthly Weather Review*, *117*(8), 1872–1890. https://doi.org/10.1175/1520-0493(1989)117,1872:POOITI.2.0.CO;2

Braun, S. A., & Tao, W.-K. (2000). Sensitivity of high-resolution simulations of Hurricane Bob (1991) to planetary boundary layer parameterizations. *Monthly Weather Review*, *128*(12), 3941–3961. https://doi.org/10.1175/1520-0493(2000)129<3941:SOHRSO>2.0.CO;2

Bryan, G. H. (2012). Effects of surface exchange coefficients and turbulence length scales on the intensity and structure of numerically simulated Hurricanes. *Mon. Wea. Rev*, *140*, 1125–1143. https://doi.org/10.1175/MWR-D-11-00231.1

Bu, Y. P., Fovell, R. G., & Corbosiero, K. L. (2017). The influences of boundary layer vertical mixing and cloud-radiative forcing on tropical cyclone size. *Journal of the Atmospheric Sciences*, *74*(4), 1273–1292. https://doi.org/10.1175/JAS-D-16-0231.1

Fischer, M. S., Rogers, R. F., & Reasor, P. (2020). An examination of local shear, vortex tilt, and tropical cyclone intensity change using airborne radar observations. *100th American Meteorological Society Annual Meeting*. Boston, MA: American Meteorological Society. Retrieved from https://ams.confex.com/ams/2020Annual/webprogram/Paper370007.html

Gopalakrishnan, S. G., Goldenberg, S., Quirino, T., Marks, F., Zhang, X., Yeh, K.-S., et al. (2012). Towards improving high-resolution numerical hurricane forecasting: Influence of model horizontal grid resolution, initialization, and physics. *Weather and Forecasting*, *27*(3), 647–666. https://doi.org/10.1175/WAF-D-11-00055.1

Gopalakrishnan, S. G., Koch, D., Upadhayay, S., DeMaria, M., Marks, F., Rappaport, E. N., et al. (2020). *2019 HFIP R&D Activities Summary: Recent Results and Operational Implementation*, Washington, DC: NATIONAL OCEANIC AND ATMOSPHERIC ADMINISTRATION United States Department of Commerce. (HFIP Technical Report: HFIP 2018-1). Retrieved from http://www.hfip.org/documents/HFIP_AnnualReport_FY2019.pdf

Gopalakrishnan, S. G., Marks, F., Zhang, X., Bao, J.-W., Yeh, K.-S., & Atlas, R. (2011). The experimental HWRF system: A study on the influence of horizontal resolution on the structure and intensity changes in tropical cyclones using an idealized framework. *Monthly Weather Review*, *139*(6), 1762–1784. https://doi.org/10.1175/2010MWR3535.12011

Gopalakrishnan, S. G., Marks, F., Zhang, J. A., Zhang, X., Bao, J.-W., & Tallapragada, V. (2013). A study of the impacts of vertical diffusion on the structure and intensity of tropical cyclones using the high resolution HWRF system. *Journal of the Atmospheric Sciences*, *70*(2), 524–541. https://doi.org/10.1175/JAS-D-11-0340.1

Gopalakrishnan, S., Srinavas, C. V., & Bhatia, K. (2016). The hurricane boundary layer. In U. C. Mohanty & S. G. Gopalakrishnan (Eds.), *Advanced numerical modeling and data assimilation techniques for tropical cyclone predictions* (pp. 589–626). Netherlands: Springer. Retrieved from https://www.springer.com/gp/book/9789402408942

Han, J. (2015). An eddy-diffusivity mass flux (EDMF) boundary layer parameterization combined with a higher-order turbulence closure model in the NCEP GFS. *27th Conference on Weather Analysis and Forecasting/23rd Conference on Numerical Weather Prediction*, Chicago: American Meteorological Society.

Han, J., & Bretherton, C. S. (2019). TKE-based moist eddy-diffusivity mass-flux (EDMF) parameterization for vertical turbulent mixing. *Weather and Forecasting*, *34*(4), 869–886. https://doi.org/10.1175/WAF-D-18-0146.1

Han, J., & Pan, H.-L. (2011). Revision of convection and vertical diffusion schemes in the NCEP Global Forecast System. *Weather and Forecasting*, *26*(4), 520–533. https://doi.org/10.1175/WAF-D-10-05038.1

Han, J. M., Witek, M. L., Teixeira, J., Sun, R., Pan, H.-L., Fletcher, J. K., & Bretherton, C. S. (2016). Implementation in the NCEP GFS of a hybrid eddy-diffusivity mass-flux (EDMF) boundary layer parameterization with dissipative heating and modified stable boundary layer mixing. *Weather and Forecasting*, *31*(1), 341–352. https://doi.org/10.1175/WAF-D-15-0053.1

Harris, L., & Lin, S. J. (2013). A two-way nested global-regional dynamical core on the cubed-sphere grid. *Monthly Weather Review*, *141*(1), 283–306. https://doi.org/10.1175/MWR-D-11-00201.1

Hawkins, H. F., & Imbembo, S. M. (1976). The structure of a small, intense hurricane—Inez 1966. *Monthly Weather Review*, *104*(4), 418–442.

Hazelton, A. T., Bender, M. A., Morin, M., Harris, L., & Lin, S.-J. (2018). 2017 Atlantic hurricane forecasts from a high-resolution version of the GFDL fvGFS model. *Weather and Forecasting*, *33*(5), 1317–1337. https://doi.org/10.1175/WAF-D-18-0056.1

Hazelton, A. T., Zhang, X., Gopalakrishnan, S., Ramstrom, W., Marks, F., & Zhang, J. A. (2020a). High-resolution ensemble HFV3 forecasts of Hurricane Michael (2018): Rapid intensification in shear. *Monthly Weather Review*, *148*(5), 2009–2032. https://doi.org/10.1175/MWR-D-19-0275.1

Hazelton, A., Zhang, Z., Liu, B., Dong, J., Alaka, G., Wang, W., et al. (2020b). 2019 Atlantic hurricane forecasts from the Global-Nested Hurricane Analysis and Forecast System: Composite statistics and key events. *Weather Forecasting*. https://doi.org/10.1175/WAF-D-20-0044.1

Hong, S.-Y., & Pan, H.-L. (1996). Nonlocal boundary layer vertical diffusion in a medium-range forecast model. *Monthly Weather Review*, *124*(10), 2322–2339.

Kepert, J. D. (2012). Choosing a boundary layer parameterization for tropical cyclone modeling. *Monthly Weather Review*, *140*(5), 1427–1445. https://doi.org/10.1175/MWR-D-11-00217.1

Lorsolo, S., Zhang, J., Marks, F. D., & Gamache, J. (2010). Estimation and mapping of hurricane turbulent energy using airborne Doppler measurements. *Monthly Weather Review*, *138*(9), 3656–3670. https://doi.org/10.1175/2010MWR3183.1

Montgomery, M. T., & Smith, R. K. (2014). Paradigms for tropical cyclone intensification. *Australian Meteorological and Oceanographic Journal*, *64*, 37–66.
Powell, M. D., Vickery, P. J., & Reinhold, T. (2003). Reduced drag coefficient for high wind speeds in tropical cyclones. *Nature*, *422*(6929), 279–283. https://www.nature.com/articles/nature01481
Reasor, P. D., Rogers, R., & Lorsolo, S. (2013). Environmental flow impacts on tropical cyclone structure diagnosed from airborne Doppler radar composites. *Monthly Weather Review*, *141*(9), 2949–2969. https://doi.org/10.1175/MWR-D-12-00334.1
Rogers, R., Lorsolo, S., Reasor, P., Gamache, J., & Marks, F. (2012). Multiscale analysis of tropical cyclone kinematic structure from airborne Doppler radar composites. *Monthly Weather Review*, *140*(1), 77–99. https://doi.org/10.1175/MWR-D-10-05075.1
Sharan, M., & Gopalakrishnan, S. G. (1997). Comparative evaluation of eddy exchange coefficients for strong and weak wind stable boundary layer modeling. *Journal of Applied Meteorology*, *36*(5), 545–559. https://doi.org/10.1175/1520-0450(1997)036<0545:CEOEEC>2.0.CO;2
Smith, R. K., Montgomery, M. T., & Sang, N. V. (2009). Tropical cyclone spin-up revisited. *Quarterly Journal of the Royal Meteorological Society*, *135*(642), 1321–1335. https://doi.org/10.1002/qj.428
Smith, R. K., & Thomsen, G. L. (2010). Dependence of tropical-cyclone intensification on the boundary layer representation in a numerical model. *Quarterly Journal of the Royal Meteorological Society*, *136*(652), 1671–1685. https://doi.org/10.1002/qj.687
Stull, R. B. (2000). *Meteorology for scientists and engineers* (2nd ed., p. 502). Pacific Grove, CA: Brooks/Cole.
Tallapragada, V., Kieu, C., Kwon, Y., Trahan, S., Liu, Q., Zhang, Z., & Kwon, I. (2014). Evaluation of storm structure from the operational HWRF model during 2012 implementation. *Monthly Weather Review*, *142*(11), 4308–4325. https://doi.org/10.1175/MWR-D-13-00010.1
Tang, J., Zhang, J. A., Aberson, S. D., Marks, F. D., & Lei, X. (2018). Multilevel tower observations of vertical eddy diffusivity and mixing length in the tropical cyclone boundary layer during landfalls. *Journal of the Atmospheric Sciences*, *75*(9), 3159–3168. https://doi.org/10.1175/JAS-D-17-0353.1
Therry, G., & Lacarrère, P. (1983). Improving the kinetic energy model for planetary boundary layer description. *Boundary-Layer Meteorology*, *25*(1), 63–88. https://doi.org/10.1007/BF00122098
Wang, W., Sippel, J. A., Abarca, S., Zhu, L., Liu, B., Zhang, Z. et al., (2018). Improving NCEP HWRF simulations of surface wind and inflow angle in the eyewall area. *Weather and Forecasting*, *33*(3), 887–898. https://doi.org/10.1175/WAF-D-17-0115.1
Yamada, T., & Mellor, G. L. (1975). A simulation of the Wangara atmospheric boundary layer data. *Journal of the Atmospheric Sciences*, *32*(12), 2309–2329. https://doi.org/10.1175/1520-0469(1975)032<2309:ASOTWA>2.0.CO;2
Zhang, J. A., Marks, F. D., Jr., Montgomery, M. T., & Lorsolo, S. (2011a). An estimation of turbulent characteristics in the low-level region of intense Hurricanes Allen (1980) and Hugo (1989). *Monthly Weather Review*, *139*(5), 1447–1462. https://doi.org/10.1175/2010MWR3435.1
Zhang, J. A., Nolan, D. S., Rogers, R. F., & Tallapragada, V. (2015). Evaluating the impact of improvements in the boundary layer parameterization on hurricane intensity and structure forecasts in HWRF. *Monthly Weather Review*, *143*(8), 3136–3155. https://doi.org/10.1175/MWR-D-14-00339.1
Zhang, J. A., Rogers, R. F., Nolan, D. S., & Marks, F. D. (2011b). On the characteristic height scales of the hurricane boundary layer. *Monthly Weather Review*, *139*(8), 2523–2535. https://doi.org/10.1175/MWR-D-10-05017.1
Zhang, J. A., Rogers, R. F., Reasor, P., Uhlhorn, E., & Marks, F. D. (2013). Asymmetric hurricane boundary layer structure from dropsonde composites in relation to the environmental vertical wind shear. *Monthly Weather Review*, *141*(11), 3968–3984. https://doi.org/10.1175/MWR-D-12-00335.1
Zhang, J. A., Rogers, R. F., & Tallapragada, V. (2017). Impact of parameterized boundary layer structure on tropical cyclone rapid intensification forecasts in HWRF. *Monthly Weather Review*, *145*(4), 1413–1426. https://doi.org/10.1175/MWR-D-16-0129.1
Zhang, J. A., & Uhlhorn, E. W. (2012). Hurricane sea surface inflow angle and an observation-based parametric model. *Monthly Weather Review*, *140*(11), 3587–3605. https://doi.org/10.1175/MWR-D-11-00339.1
Zhang, Z., Tallapragada, V., Kieu, C., Trahan, S., & Wang, W. (2014). HWRF based ensemble prediction system using perturbations from GEFS and stochastic convective trigger function. *Tropical Cyclone Research and Review*, *3*, 145–161.